Electronic Supplementary Material (ESI) for ChemComm.

Electronic Supporting Information

Polymorph Driven Diversification of Photosalient Responses in a Zinc(II) Coordination Complex

Victoria N.P. Pham-Tran, James G.D. Moffat, Katherine M. Marczenko*[a]

[a]Department of Chemistry, Carleton University, Ottawa, ON, Canada

Email: katherinemarczenko@cunet.carleton.ca

Contents

1 General

Synthetic Procedures

Manipulations were performed in air under standard atmospheric conditions. All deuterated solvents were dried and stored over activated molecular sieves (3 Å).

Solution NMR Spectroscopy

All Nuclear Magnetic Resonance (NMR) experiments were carried out on a Bruker AV-300 spectrometer in dried deuterated solvent. Residual ^{1}H signal of the deuterated solvent was used for chemical shift calibration of the respective experiments. The NMR data were processed using Bruker TopSpin 4.3.0.[1]

Powder X-Ray Diffraction

Powder X-Ray Diffraction (PXRD) data were collected using a PANalytical Empyrean diffractometer in a reflection (Bragg-Brentano) geometry with Cu K_α radiation source, Ni K_β filter and PIXcel1D linear detector. Powder diffractograms were recorded in the 5-50° 2θ range with a step size of 0.01303°. Data collection was controlled with X'Pert Data Collector Software.[2]

Single-Crystal X-Ray Diffraction

Single-Crystal X-Ray Diffraction (SCXRD) experiments were run on a Rigaku MiniLab II diffractometer, equipped with a Mo source (λ = 0.71 Å) and Oxford 800 cryostream. Reflections were integrated using the CrysAlias Pro software (v43).[3] The structures were solved by intrinsic phasing and a full matrix least-squares refinement was carried out using all data in Olex2-1.5.[4] Non-hydrogen atoms were refined anisotropically, while hydrogen atoms were added in calculated positions. The crystallographic data 1-Form-III at 115 K (LT), 1-Form-III at 293 K (RT), 1-Form-III' at 115 K (LT), 1-Form-III' at 293 K (RT) and compound (2) at 115 K (LT) are shown in Table S1 and S2. CIFs have been deposited to the Cambridge Crystallographic Data Centre (CCDC) with deposition numbers 2346070-2346074.

UV-VIS Spectroscopy

Solution UV-VIS spectra (Figure S8) were obtained on a Shimadzu UV-2450 instrument using a high-performance single monochromator and an R-928 photomultiplier tube. A single baseline scan from 260-900 nm was performed on a 0.1 cm quartz cuvette containing the sample solvent. Sample and baseline data acquisition was performed at a 1 nm resolution set to a 'Medium' scan speed.

Solid-state UV-VIS spectra (Figure S9) were obtained on an Agilent Cary 100 UV-VIS using a Labsphere-DRA (Diffuse Reflectance Accessory)-CA-30I integrating sphere. A baseline and 0% transmittance scan from 350-700 nm were performed before sample data acquisition. The baseline scan was taken of 2 sandwiched 1 mm quartz slides, and the 0% transmittance scan was performed on an opaque surface blocking the source.

Emission Spectroscopy

Fluorescence spectra (Figure S10) were obtained on Shimadzu RF-1501 spectrofluorophotometer using 150 W Xenon lamp with ozone resolving-type lamp housing. All samples were sandwiched between two (51 mm x 51 mm x 0.5 mm) glass slides.

Vibrational Spectroscopy

Infrared spectra (Figure S11) were obtained on an Agilent Cary 630 FTIR ZnSe engine instrument equipped with a single-bounce diamond ATR sampling accessory, a standard globar source, and a DLaTGS detector.

Differential Scanning Calorimetry

DSC experiments (Figures S12, S13) were performed on a TA Instruments Q10 model. The DSC was calibrated at the melting point of the indium metal (156.6 °C). All DSC samples were hermetically sealed in aluminum pans prior to analysis. All samples were heated to 400 °C with a ramp rate of 10 °C min^{-1}, using air as the purge gas. The melting points were measured at the peak of the endothermic process.

Commercial Reagents

Triethyl phosphite (98%), 1-(chloromethyl)naphthalene (90%), and n-butyllithium (1.6 M in hexanes) were obtained from Sigma Aldrich. Triethylamine (reagent) was received from Fisher Chemical. 4-pyridinecarboxaldehyde was obtained from Thermo Scientific. $Zn(NO_3)_2{\cdot}6H_2O$ was obtained from Fisher Scientific. and 4-hydroxybenzoic acid was obtained from TCI America.

Starting Materials

(E)-4-(1-naphthylvinylpyridine) was synthesized according to the procedure outlined by Marczenko *et. al*.[5]

Synthetic Procedure

Synthesis of Form III: A solution of $Zn(NO_3)_2{\cdot}6H_2O$ (0.069 g, 0.230 mmol) in deionized water (1 mL) was prepared in a 4-dram vial. A solution of 4-nvp (0.103 g, 0.447 mmol) in MeOH (2 mL) was slowly layered on top of the $Zn(NO_3)_2{\cdot}6H_2O$ solution, affording an off-white precipitate upon solution contact. This was immediately followed by layering of a 4-ohbz (0.064 g, 0.466 mmol) solution, neutralized with NEt_3 (65.4 µL, 0.466 mmol), in EtOH (2 mL). The 3-layer solution was wrapped in foil and moved to a low light environment for 4 days. This afforded a light yellow precipitate of $Zn(4\text{-ohbz})_2(4\text{-nvp})_2$ (0.107 g, 59.5% yield). ^{1}H-NMR (DMSO, 300 MHz): 9.85 (2H, s), 8.60 (4H, d, *J* = 6 Hz), 8.46 (2H, d, *J* = 8 Hz), 8.38 (2H, d, *J* = 16 Hz), 7.91-8.02 (6H, m), 7.73-7.83 (8H, m), 7.53-7.66 (6H, m), 7.32 (2H, d, *J* = 16 Hz), 6.74 (4H, d, *J* = 9 Hz).

$$Zn(NO_3)_2{\cdot}6H_2O + 2\ (4\text{-ohbz}) + 2\ (4\text{-nvp}) + 2\ NEt_3 \longrightarrow Zn(4\text{-ohbz})_2(4\text{-nvp})_2 + 2\ HNEt_3NO_3$$

2 Powder X-ray Diffraction

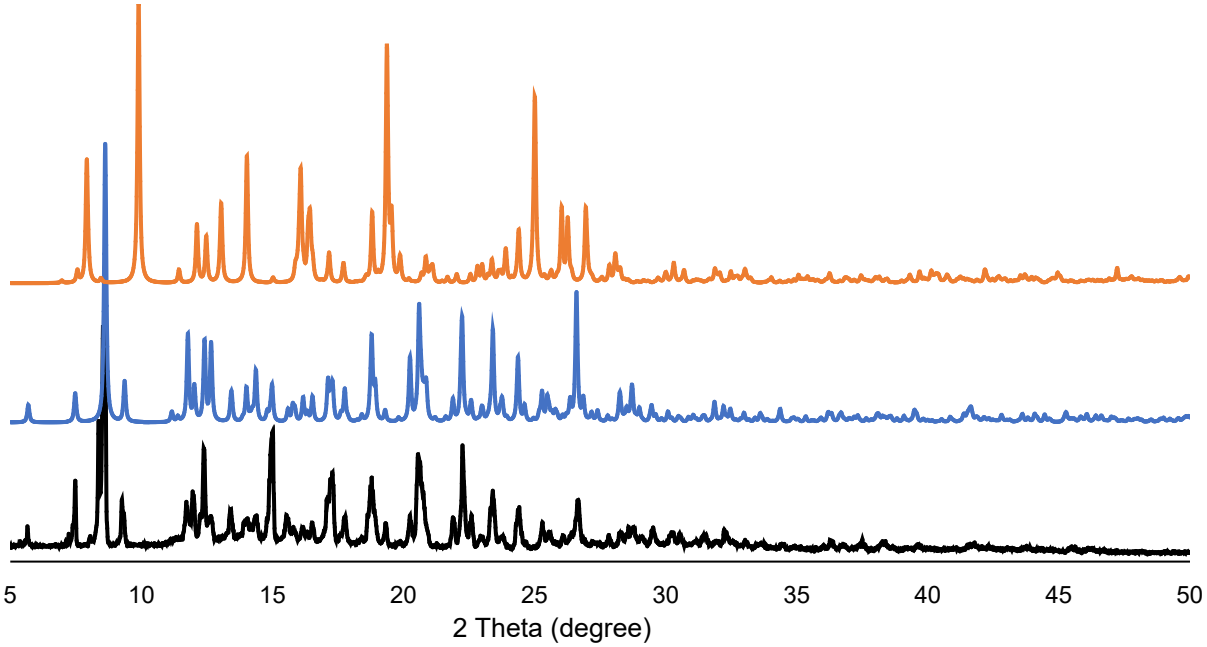

Figure S1. Powder X-ray Diffraction pattern of **1-Form-III** (experimental, black; calculated, blue) and **1-Form-I** (calculated, orange) at 293 K.

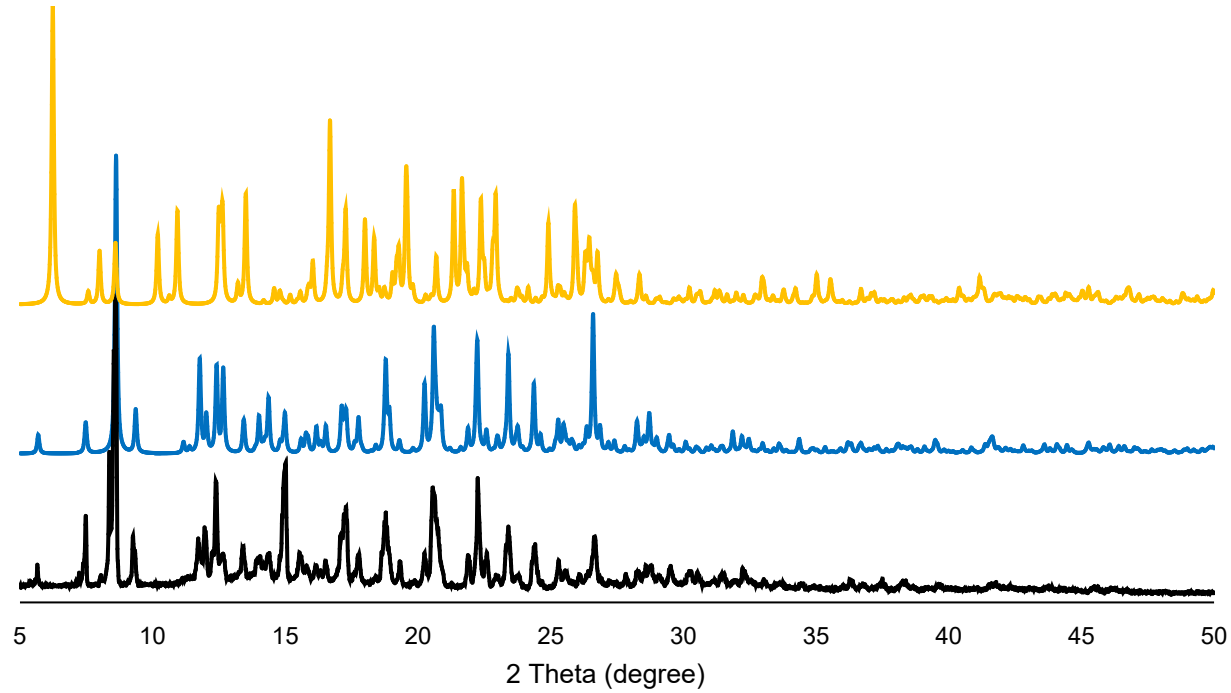

Figure S2. Powder X-ray Diffraction pattern of **1-Form-III** (experimental, black; calculated, blue) at 293 K and **1-Form-II** (calculated, yellow) at 100 K.

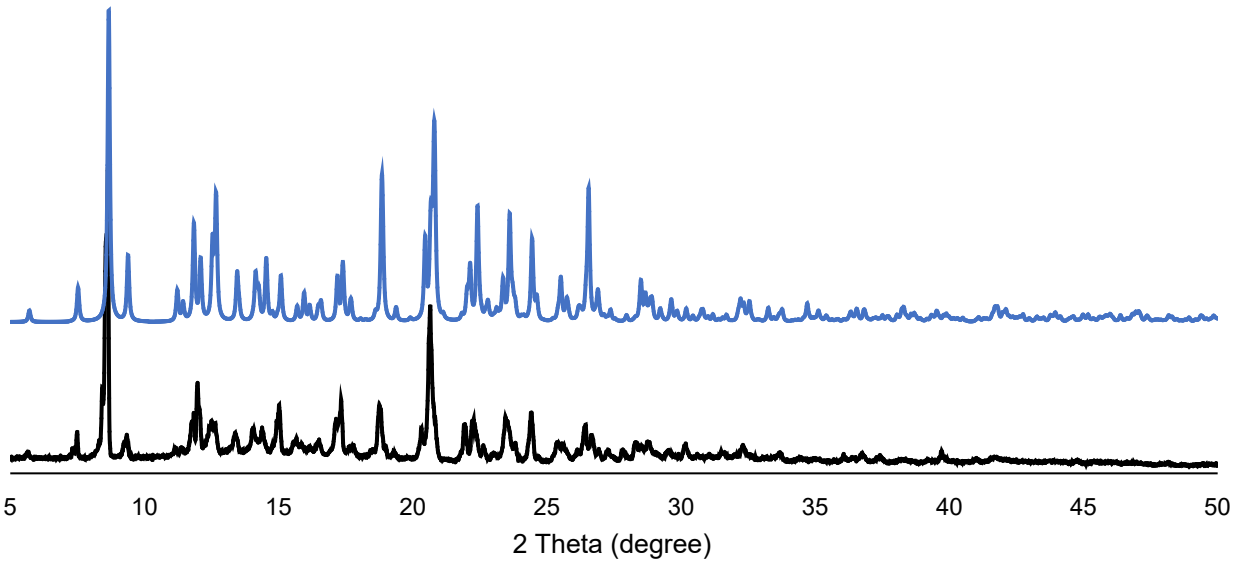

Figure S3. Powder X-ray Diffraction pattern of **2** (experimental, black; calculated, blue) at 293 K.

3 Variable-Cell Powder Difference Method (VC-xPWDF)

Table S1. VC-XPWDF scores for the comparison of SCXRD structures with experimentally obtained PXRD patterns for various phases at room-temperature. VC-xPWDF score < 0.10 is considered a possible matching structure.[8]

SCXRD Structure	PXRD Pattern	VC-xPWDF
1-Form-I_RT[a]	**1-Form-III**_RT[b]	0.4370
1-Form-II_LT[a]	**1-Form-III**_RT[b]	0.1525
1-Form-III_RT[b]	**1-Form-III**_RT[b]	0.0496
Compound **2**_RT[c]	Compound **2**_RT[b]	0.0751

[a]Published by Mir *et. al.*, CCDC #2214421.[6]
[b]Reported within.
[c]Published by Mir *et. al.*, CCDC #2214423.[6]

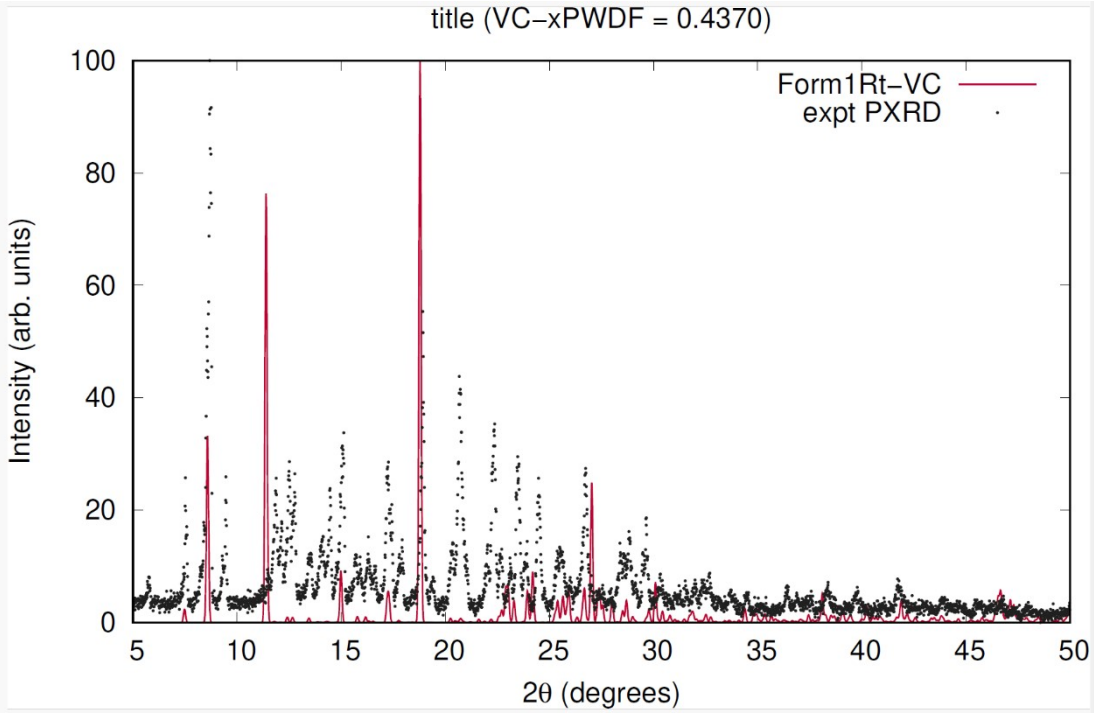

Figure S4. Overlay of calculated powder diffractogram of **1-Form-I** (red line) with experimentally obtained PXRD data (black dot) from attempted 1:1:1:1 recrystallization experiments at 293 K. VC-xPWDF score of 0.4370 was obtained.

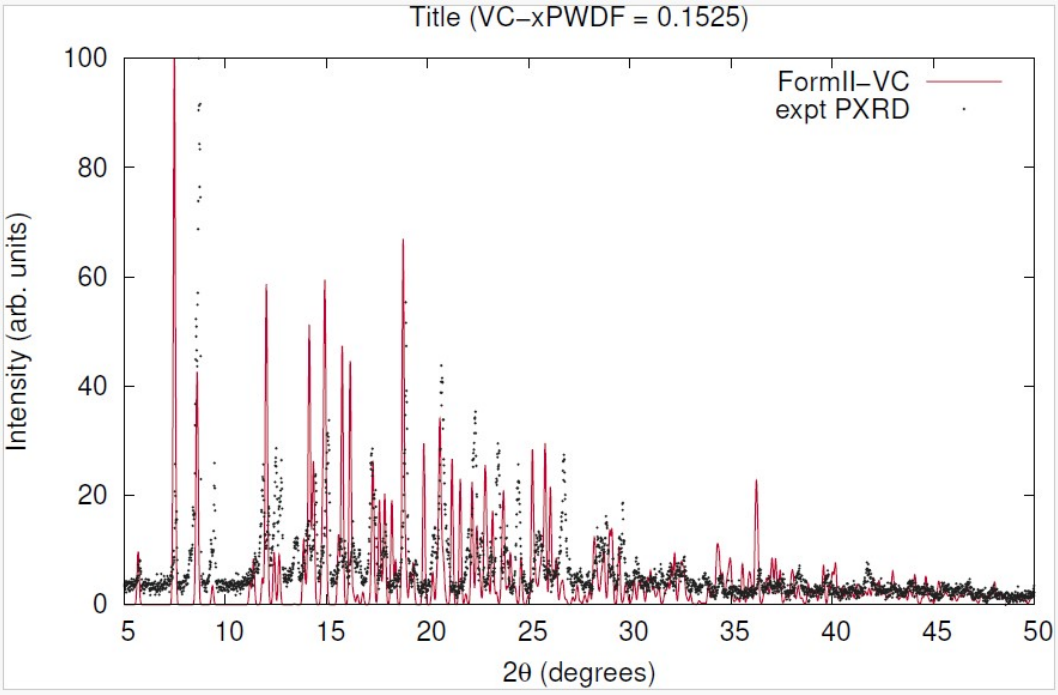

Figure S5. Overlay of calculated powder diffractogram of **1-Form-II** (red line) with experimentally obtained PXRD data (black dot) from attempted 1:1:1:1 recrystallization experiments at 293 K. VC-xPWDF score of 0.1525 was obtained.

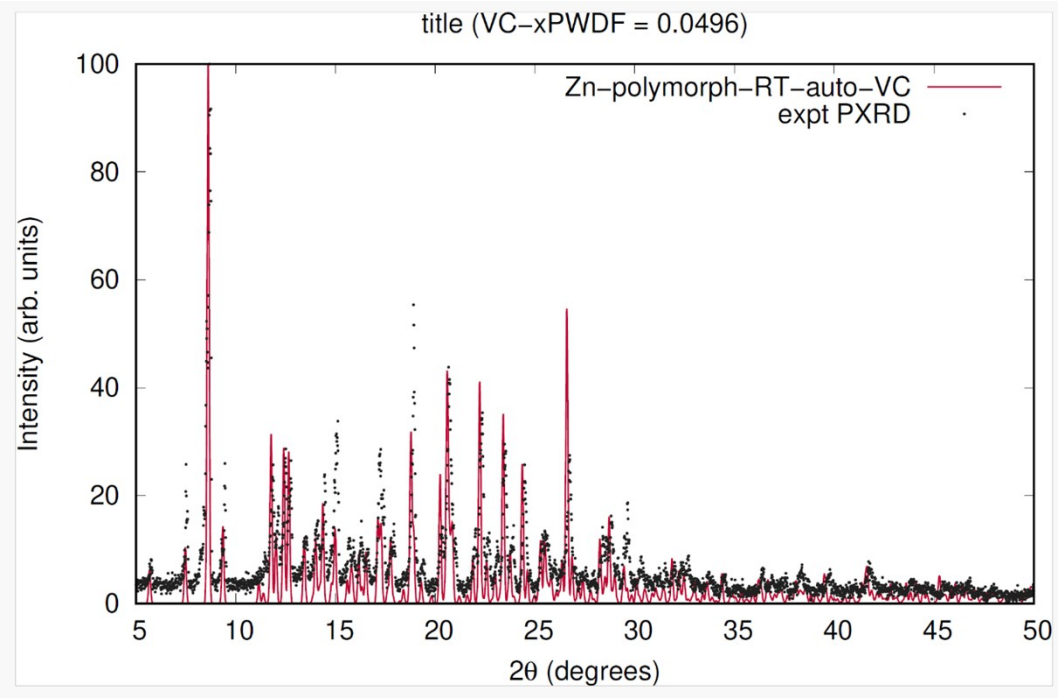

Figure S6. Overlay of calculated powder diffractogram of **1-Form-III** (red line) with experimentally obtained PXRD data (black dot) of **1-Form-III** at 293 K. VC-xPWDF score of 0.0496 was obtained.

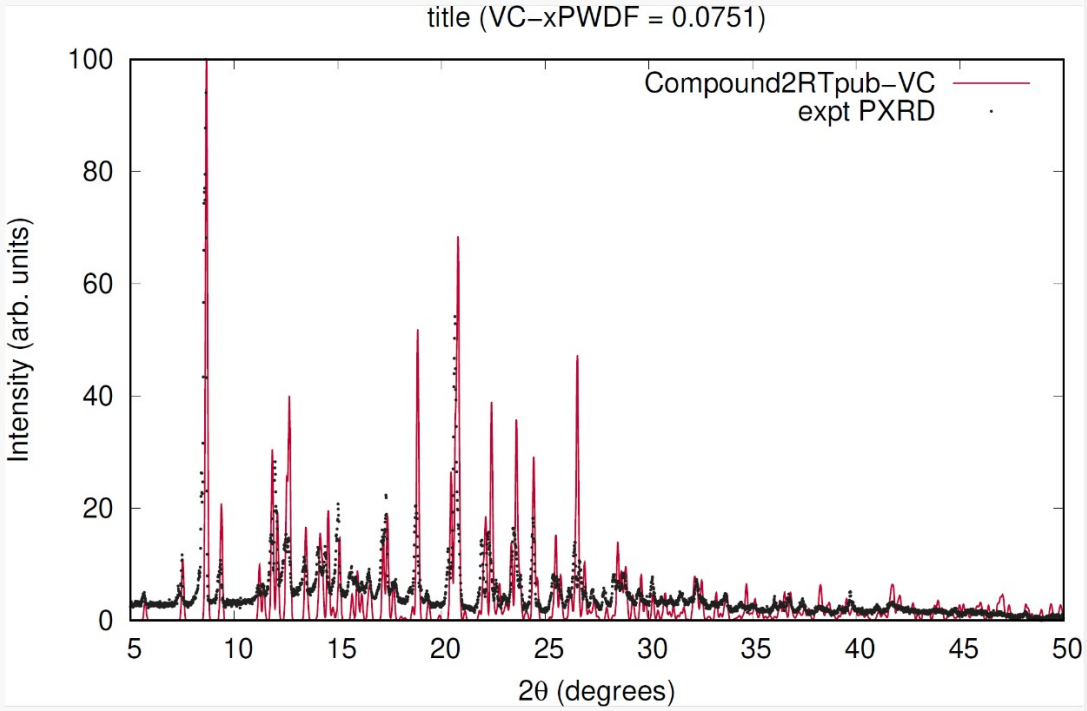

Figure S7. Overlay of calculated powder diffractogram of **2** (red line) with experimentally obtained PXRD data (black dot) of **2** at 293 K. VC-xPWDF score of 0.0751 was obtained.

4 Spectroscopy

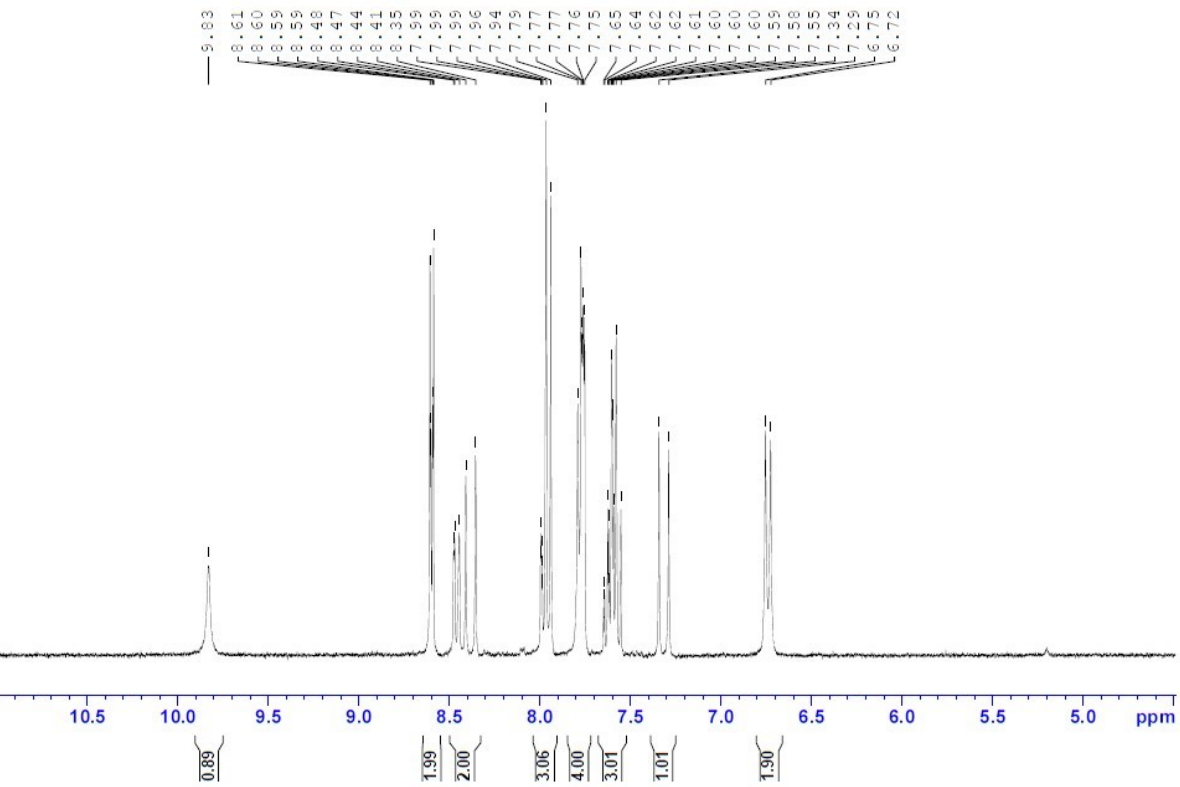

*

Figure S8. ^{1}H NMR (300 MHz; dimethyl sulfoxide-d_6) of **1-Form-III**. The peak at 5.20 ppm (marked with *) corresponds to the cyclobutane peak of (**2**) and indicates partial dimerization of **1-Form-III** even in ambient light. Normalization of the sum of integrals for the peak at 5.20 ppm and the olefin protons at 6.72 ppm yield relative ratios of 1.9:98:1, respectively, indicating conversion of 2%.

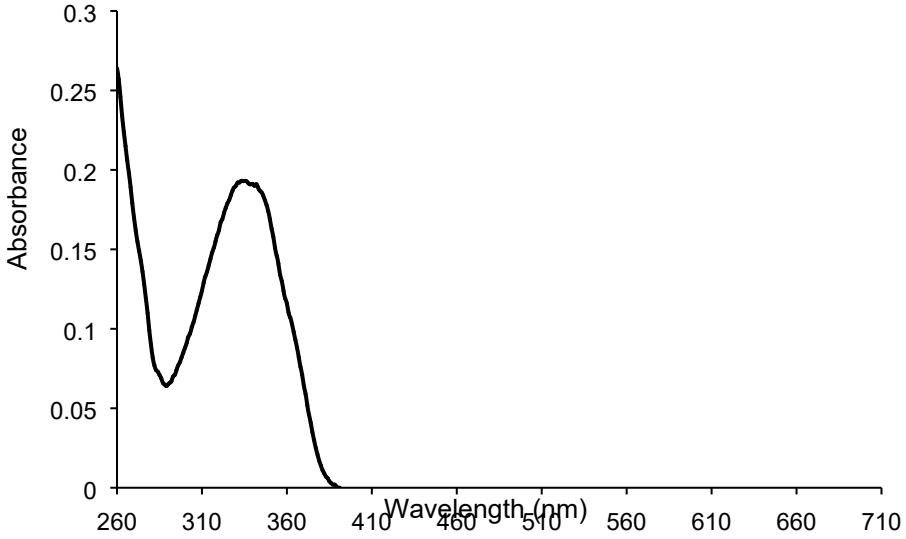

Figure S9. Blank corrected UV-Vis spectrum of a 5.08×10^{-5} M solution of $Zn(4\text{-ohbz})_2(4\text{-nvp})_2$ in DMSO (λ_{max} = 340 nm).

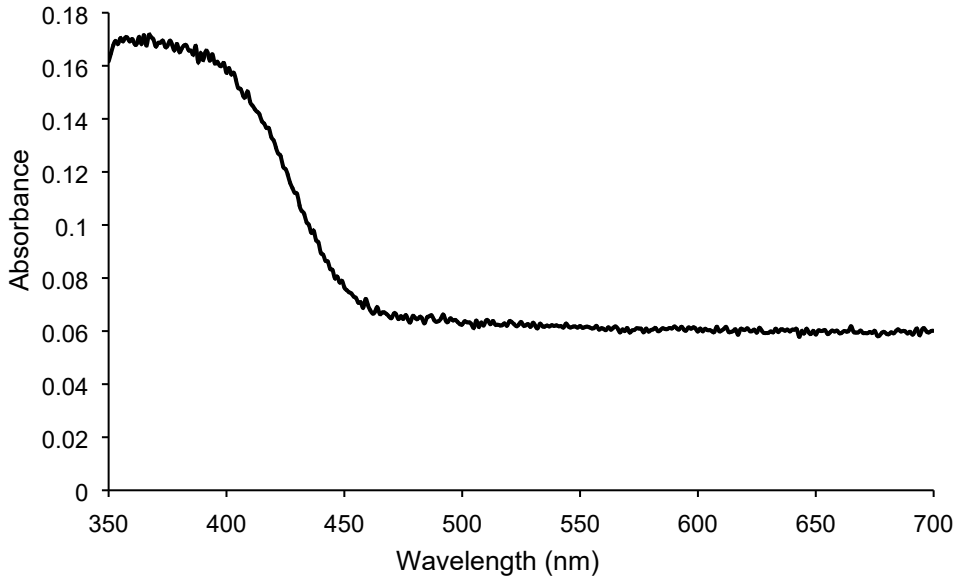

Figure S10. UV-Vis spectrum of a solid **1-Form-III** (λ_{max} = 365 nm).

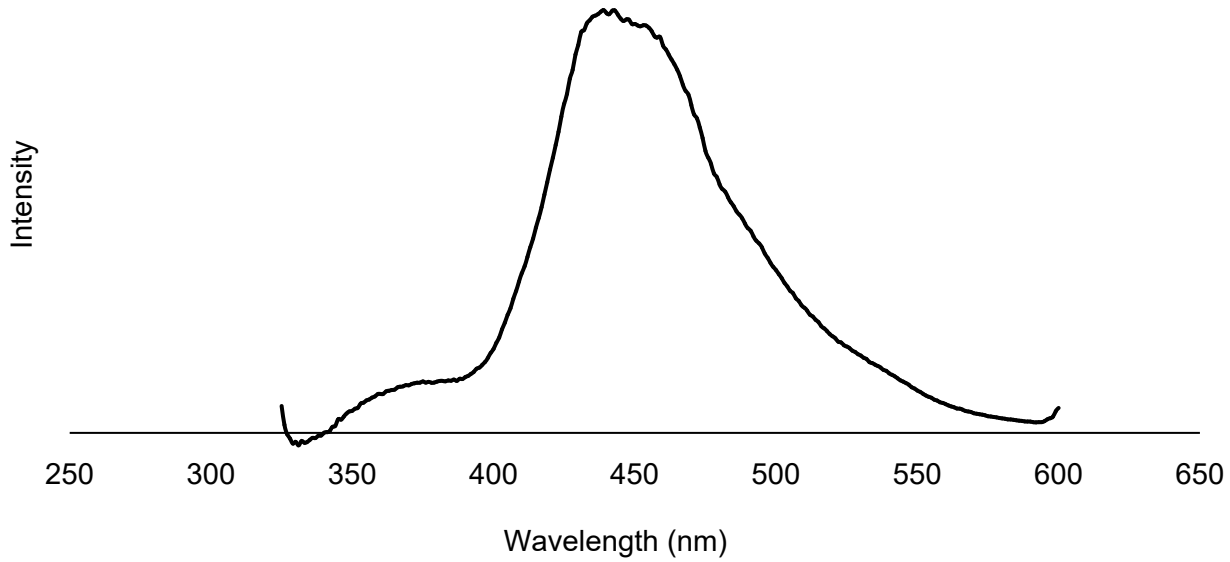

Figure S11. Emission spectrum of solid **1-Form-III** using an excitation wavelength of 350 nm (λ_{max} = 445 nm).

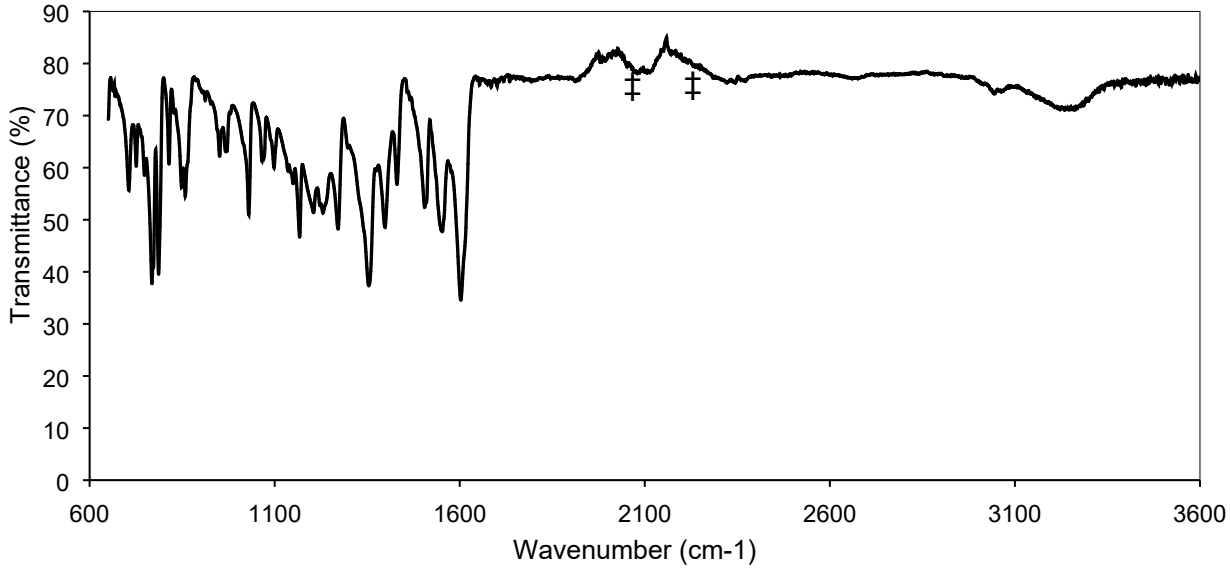

Figure S12. FTIR spectrum of **1-Form-III**, acquired from 64 scans at 2 cm^{-1} resolution for both background and sample measurements. A Happ Genzel apodization and Mertz phase correction was applied. The symbol ‡ indicates artifacts from the diamond ATR crystal.[7]

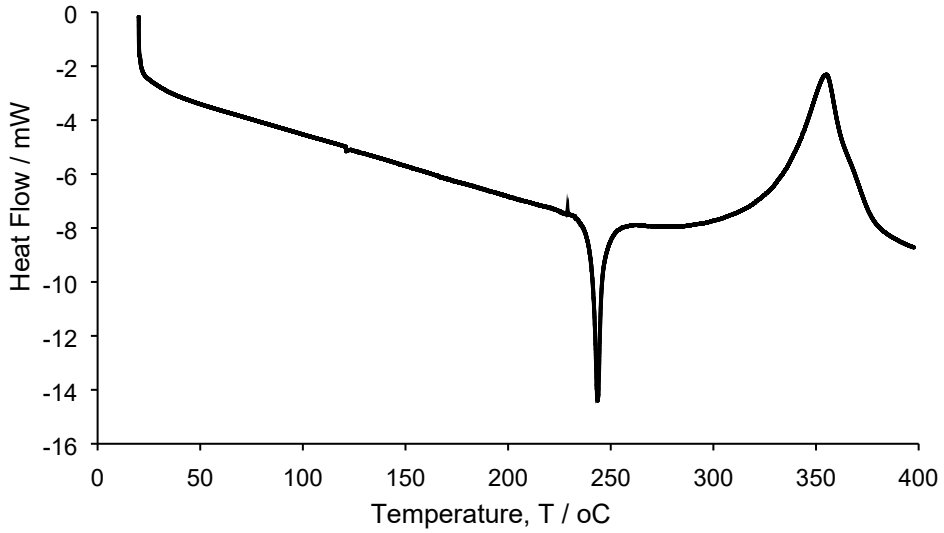

Figure S13. DSC thermogram of **1-Form-III**. A sample size of 1.6 mg and ramp rate of 5.00 °C /min from room temperature (20.05 °C) to 400.00 °C was used.

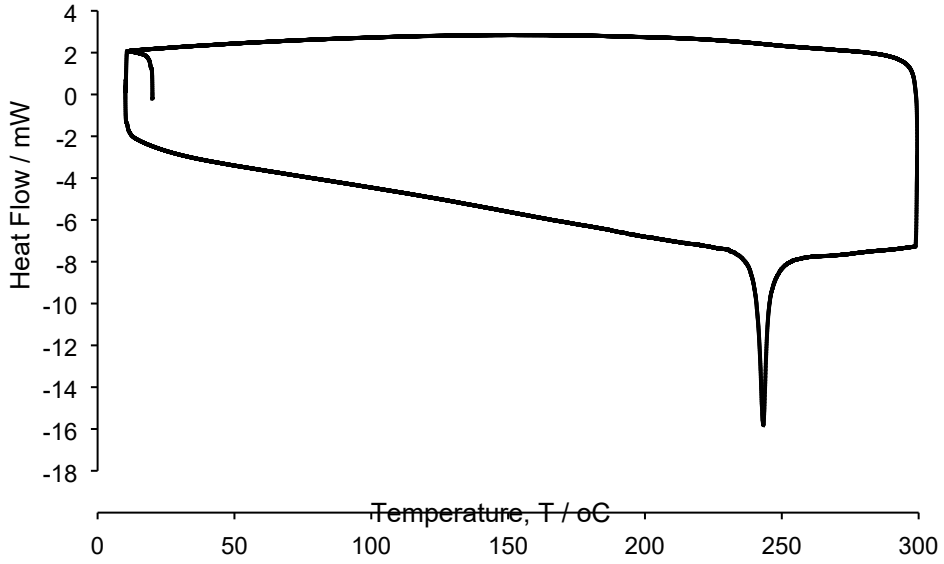

Figure S14. DSC thermogram of **1-Form-III**. A sample size of 1.7 mg was used. The following program was used: 5.00 °C /min ramp to 10.00 °C /min, isothermal for 1.00 min, 5.00 °C /min ramp to 300.00 °C, isothermal for 1.00 min, 5.00 °C /min ramp to 10.00 °C.

5 X-ray Crystallography

Table S2. Crystal data and refinement parameters for **1-Form-III** at 115 K (LT), **1-Form-III** at 293 K (RT), and **1-Form-III'** at 115 K (LT).

	1-Form-III_LT	**1-Form-III_RT**	**1-Form-III'_LT**
Identification code	1-Form-III_LT	1-Form-III	1-Form-III'_LT
Empirical formula	$C_{48}H_{36}N_2O_6Zn$	$C_{48}H_{36}N_2O_6Zn$	$C_{48}H_{36}N_2O_6Zn$
Formula weight	802.226	802.16	802.226
Temperature/K	114.98(15)	293.1(5)	115.0(2)
Crystal system	Monoclinic	Monoclinic	Monoclinic
Space group	$P2_1/c$	$P2_1/c$	$P2_1/c$
a/Å	7.8902(1)	7.8927(3)	7.8858(2)
b/Å	23.5724(4)	23.5873(7)	23.5060(7)
c/Å	20.3308(4)	20.5265(6)	20.4093(7)
α/°	90	90	90
β/°	92.206(2)	91.988(3)	91.544(3)
γ/°	90	90	90
Volume/Å^3	3778.54(11)	3819.1(2)	3781.8(2)
Z	4	4	4
ρ_{calc}g/cm^3	1.410	1.395	1.409
μ/mm^{-1}	0.706	0.698	0.706
F(000)	1664.0	1664.0	1664.0
Crystal size/mm^3	0.359 × 0.199 × 0.1	0.471 × 0.162 × 0.127	0.281 × 0.186 × 0.051
Radiation/Å	Mo Kα (λ = 0.71073)	Mo Kα (λ = 0.71073)	Mo Kα (λ = 0.71073)
2Θ range for data collection/°	5.16 to 56.0	3.97 to 52.766	4 to 50
Index ranges	-11 ≤ h ≤ 11, -33 ≤ k ≤ 33, -29 ≤ l ≤ 29	-9 ≤ h ≤ 9, -29 ≤ k ≤ 29, -25 ≤ l ≤ 25	-11 ≤ h ≤ 11, -26 ≤ k ≤ 33, -29 ≤ l ≤ 29
Reflections collected	128060	28141	67982
Independent reflections	9132 [R_{int} = 0.0811, R_{sigma} = 0.0587]	7780 [R_{int} = 0.0308, R_{sigma} = 0.0397]	6668 [R_{int} = 0.1355, R_{sigma} = 0.1879]
Data/restraints/parameters	9132/49/565	7780/564/589	6668/377/652
Goodness-of-fit on F^2	1.070	1.083	1.139
Final R indexes [I>=2σ (I)][a,b]	R_1 = 0.0463, wR_2 = 0.0816	R_1 = 0.0460, wR_2 = 0.0854	R_1 = 0.0876, wR_2 = 0.1337
Final R indexes [all data][a,b]	R_1 = 0.0664, wR_2 = 0.0871	R_1 = 0.0678, wR_2 = 0.0916	R_1 = 0.1334, wR_2 = 0.1473
Largest diff. peak/hole / e Å^{-3}	0.54/-0.59	0.21/-0.31	1.31/-1.21

a $$R_1 = \frac{\Sigma|F_o - F_c|}{\Sigma|F_o|}$$

b $$wR_2 = \sqrt{\frac{\Sigma w(F_o - F_c)^2}{\Sigma w(F_o)^2}}$$

Table S3. Crystal data and refinement parameters for **1-Form-III'** at 293 K (RT) and compound (**2**) at 115 K (LT).

	1-Form-III'_RT	**2_LT**
Identification code	1-Form-III'	Compound2_LT
Empirical formula	$C_{48}H_{36}N_2O_6Zn$	$C_{96}H_{72}N_4O_{12}Zn_2$
Formula weight	802.16	1604.31
Temperature/K	292.7(3)	115.0(2)
Crystal system	Monoclinic	Monoclinic
Space group	$P2_1/c$	$P2_1/c$
a/Å	7.9164(2)	7.9091(2)
b/Å	23.6249(8)	23.3932(6)
c/Å	20.5918(6)	20.4994(5)
α/°	90	90
β/°	91.802(3)	90.281(2)
γ/°	90	90
Volume/Å^3	3849.3(2)	3792.74(16)
Z	4	4
ρ_{calc}g/cm^3	1.384	1.405
μ/mm^{-1}	0.693	0.703
F(000)	1664.0	1664
Crystal size/mm^3	0.491 × 0.174 × 0.110	0.284 × 0.137 × 0.055
Radiation/Å	Mo Kα (λ = 0.71073)	Mo Kα (λ = 0.71073)
2Θ range for data collection/°	3.976 to 52.826	3.98 to 56
Index ranges	-9 ≤ h ≤ 9, -29 ≤ k ≤ 29, -25 ≤ l ≤ 25	-11 ≤ h ≤ 11, -33 ≤ k ≤ 33, -29 ≤ l ≤ 29
Reflections collected	27701	75193
Independent reflections	7862 [R_{int} = 0.0476, R_{sigma} = 0.0662]	9157 [R_{int} = 0.0789, R_{sigma} = 0.0918]
Data/restraints/parameters	7862/550/595	9157/0/516
Goodness-of-fit on F^2	1.036	1.062
Final R indexes [I>=2σ (I)][a,b]	R_1 = 0.0551, wR_2 = 0.1063	R_1 = 0.0542, wR_2 = 0.0830
Final R indexes [all data][a,b]	R_1 = 0.0982, wR_2 = 0.1189	R_1 = 0.0914, wR_2 = 0.0917
Largest diff. peak/hole / e Å^{-3}	0.45/-0.32	0.66/-0.85

a $$R_1 = \frac{\Sigma|F_o - F_c|}{\Sigma|F_o|}$$

b $$wR_2 = \sqrt{\frac{\Sigma w(F_o - F_c)^2}{\Sigma w(F_o)^2}}$$

Table S4. Summary of crystallographic parameters of **1-Form-I** and **1-Form-III**, before ("*Before UV*"), during ("*Cracks*"), and after irradiation ("*Complete*"). Data for **1-Form-III** is show at 115 K and 293 K.

1-Form-I – 293 K	Before UV	After UV Irradiation	
		Cracks[a]	Complete[b]
a (Å)	22.9098(16)	22.6733(13)	7.8757(2)
b (Å)	15.4421(10)	15.4419(4)	23.4713(8)
c (Å)	22.7056(14)	22.7005(8)	20.5487(8)
b (º)	103.122(7)	103.606(4)	90.977(3)
Volume (Å^3)	7823.3(9)	7724.8(6)	3797.9(3)
V/Z (Å^3/molecule)	977.91(1)	965.60(1)	949.48(1)
∆V/Z (Å^3/molecule)	-	-1.26%	-2.90%
1-Form-III – 293 K	Before UV	After UV Irradiation	
		Cracks[c]	Complete[b]
a (Å)	7.8927(3)	7.9164(2)	7.8757(2)
b (Å)	23.5873(7)	23.6249(8)	23.4713(8)
c (Å)	20.5265(6)	20.5918(6)	20.5487(8)
b (º)	91.988(3)	91.802(3)	90.977(3)
Volume (Å^3)	3819.1(2)	3849.3(2)	3797.9(3)
V/Z (Å^3/molecule)	954.75(1)	962.33(1)	949.48(1)
∆V/Z (Å^3/molecule)	-	+0.79%	-0.56%
1-Form-III – 115 K	Before UV	After UV Irradiation	
		Cracks[c]	Complete[b]
a (Å)	7.8902(1)	7.8858(2)	7.9091(2)
b (Å)	23.5724(4)	23.5060(7)	23.3932(6)
c (Å)	20.3308(4)	20.4093(7)	20.4994(5)
b (º)	92.206(2)	91.544(3)	90.281(2)
Volume (Å^3)	3778.54(11)	3781.8(2)	3792.74(16)
V/Z (Å^3/molecule)	944.64(1)	945.45(1)	948.19(1)
∆V/Z (Å^3/molecule)	-	+0.09%	+0.38%

[a]Represents the structural data obtained for **1-Form-I'**. [b]Represents the structural data obtained for (**2**). [c]Represents the structural data obtained for **1-Form-III'**.

$$\Delta X\ (\%) = \frac{(V_2 - V_1)}{|V_1|} \times 100$$

Equation S1. Percent change was calculated according to the above equation, where V_1 is value 1 and V_2 is value 2, and ΔX is the calculated change value in percent.

Table S5. Replication of **Table 1** from main text with full error analysis. Summary of cell lengths (*a*, *b*, *c*; Å) and angles (β, °) of 1-Form-I, 1-Form-III, before, during, and after irradiation, where Δ represents the percent change along a specified parameter (Equation S1). V/Z is the unit cell volume/molecule ratio (Å^3/molecule). Partial conversion represents transformation of **1-Form-X** to **1-Form-X'** (X= I, III). Complete conversion represents transformation of **1-Form-X** to (**2**) (X= I, III). The percent change from **1-Form-I** to (**2**) was not tracked due to significant changes in the unit cell.

Conversion	Species	Δ*a*(%)	Δ*b*(%)	Δ*c*(%)	Δ*β*(%)	Δ*V*/*Z*(%)
Partial	1-Form-I-RT	–1.034 ± 0.009	–0.001 ± 0.007	–0.022 ± 0.007	+0.469 ± 0.008	–1.26 ± 0.01
	1-Form-III-RT	+0.300 ± 0.005	+0.159 ± 0.005	+0.318 ± 0.004	–0.202 ± 0.005	+0.791 ± 0.007
	1-Form-III-LT	–0.056 ± 0.003	–0.282 ± 0.003	+0.386 ± 0.004	–0.718 ± 0.004	+0.086 ± 0.006
Complete	1-Form-I-RT	-	-	-	-	–2.90 ± 0.01
	1-Form-III-RT	–0.215 ± 0.005	–0.492 ± 0.004	–0.108 ± 0.005	–1.099 ± 0.005	–0.555 ± 0.009
	1-Form-III-LT	+0.240 ± 0.003	–0.760 ± 0.003	+0.829 ± 0.003	–2.088 ± 0.003	+0.376 ± 0.005

$$\Delta R = \sqrt{\left(\frac{\partial R}{\partial V_1}\Delta V_1\right)^2 + \left(\frac{\partial R}{\partial V_2}\Delta V_2\right)^2}$$

$$\Delta R = \sqrt{\left(\frac{-V_2}{{V_1}^2}\Delta X\right)^2 + \left(\frac{1}{V_1}\Delta V_2\right)^2}$$

Equation S2. Formula used for propagation of uncertainty in **Table S4**.

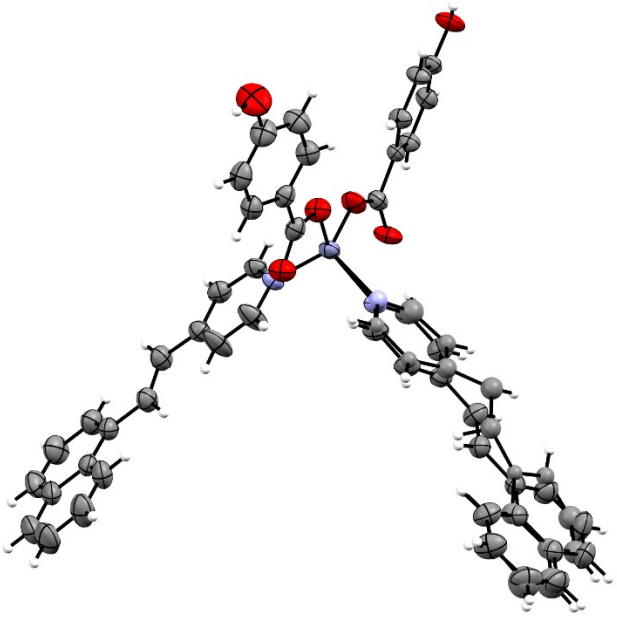

Figure S15. Single crystal x-ray structure of **1-Form-III_RT**. The asymmetric unit is shown and thermal ellipsoids are drawn at the 50% probability level.

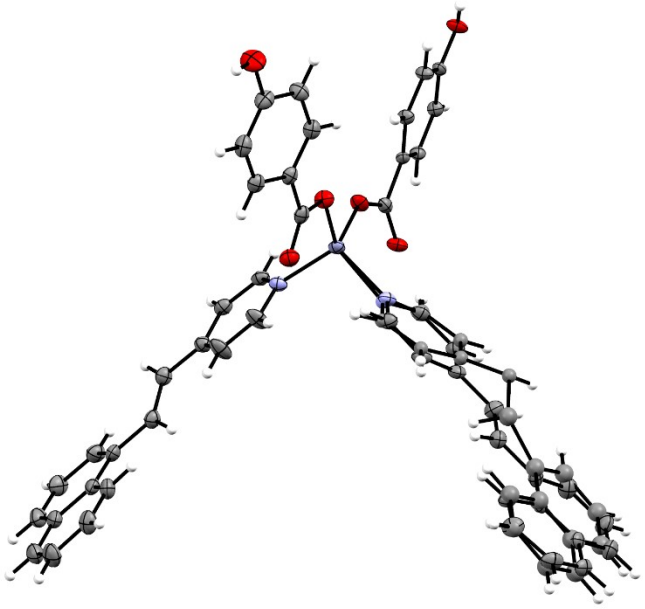

Figure S16. Single crystal x-ray structure of **1-Form-III_LT**. The asymmetric unit is shown and thermal ellipsoids are drawn at the 50% probability level.

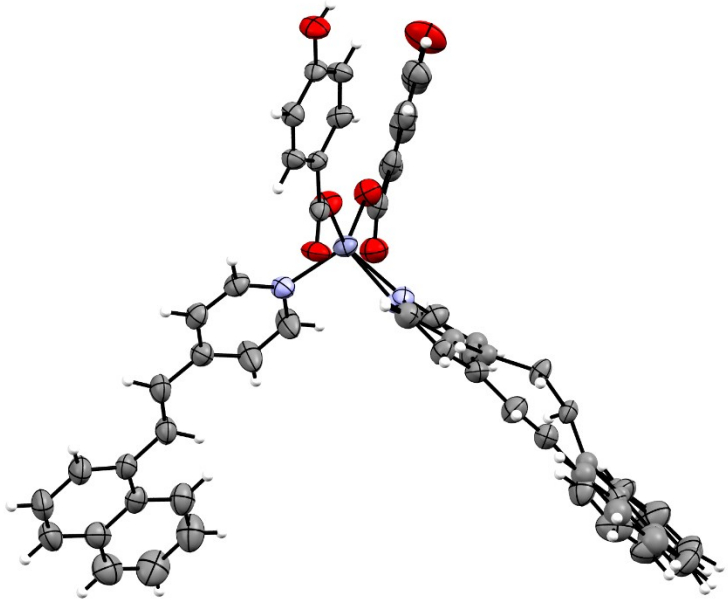

Figure S17. Single crystal x-ray structure of **1-Form-III'_RT**. The asymmetric unit is shown and thermal ellipsoids are drawn at the 50% probability level.

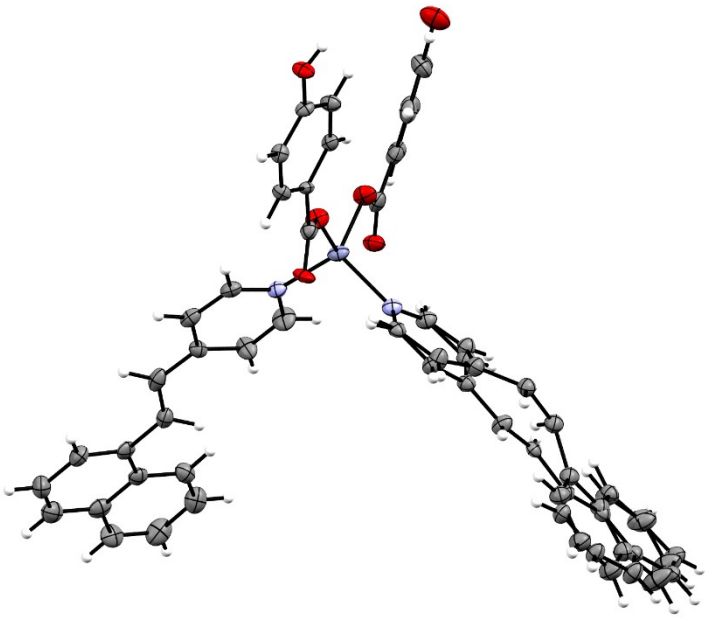

Figure S18. Single crystal x-ray structure of **1-Form-III'_LT**. The asymmetric unit is shown and thermal ellipsoids are drawn at the 50% probability level.

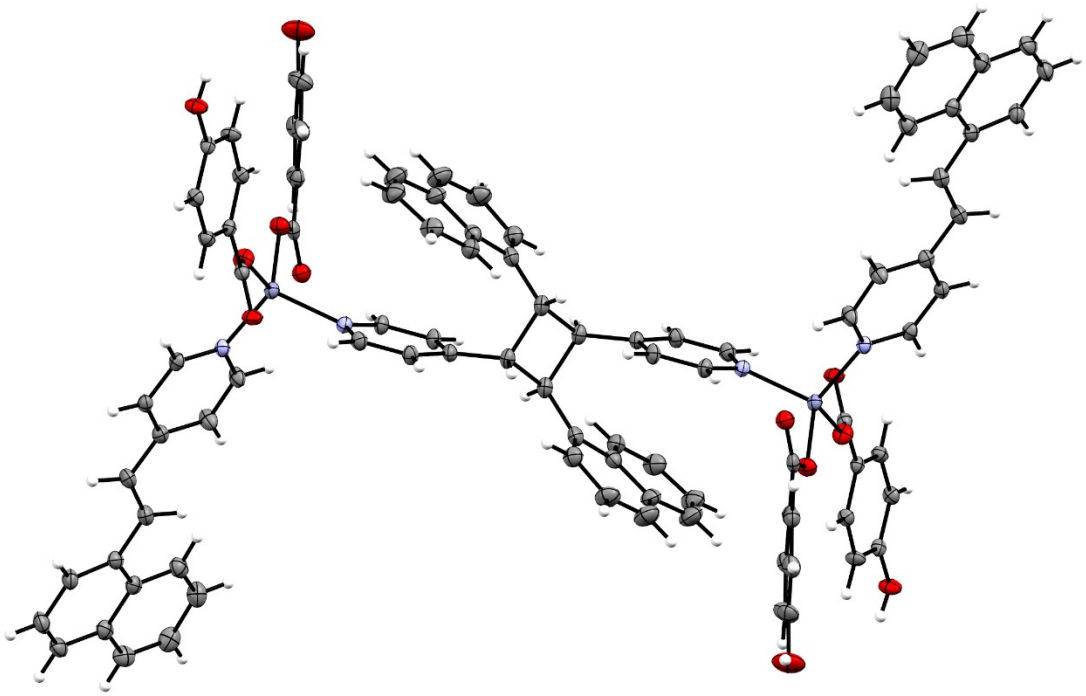

Figure S19. Single crystal x-ray structure of **Compound 2** at 115 K. Thermal ellipsoids are drawn at the 50% probability level.

6 Optical Microscopy

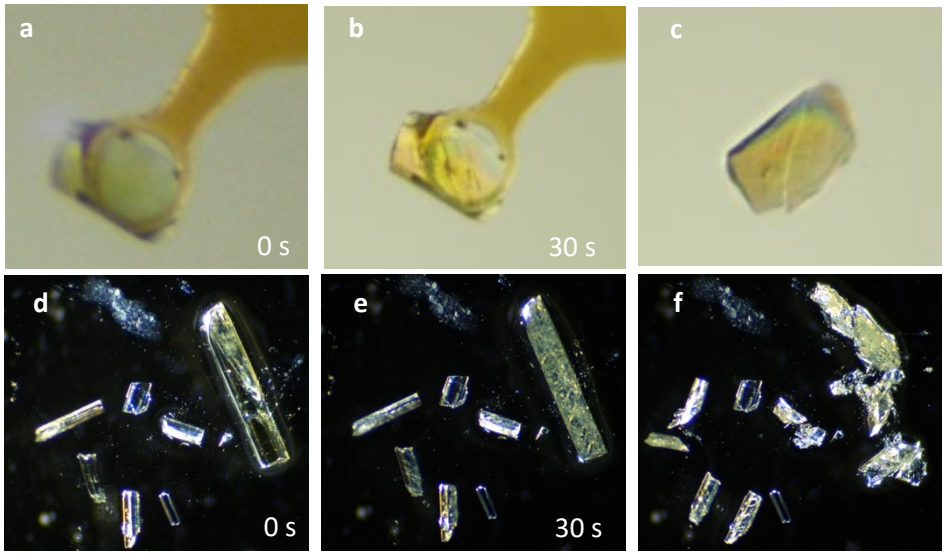

Figure S20. A series of photographs of the photosalient effect observed by optical microscopy using a 1-Watt (a-c) light source and 10-Watt (d-f) light source. The images were taken (**a**, **d**) before UV-light irradiation and (**b**, **e**) after 30 seconds of UV-light irradiation. Crystals in images (**c**, **f**) were gently poked to show the degree of fragmentation present.

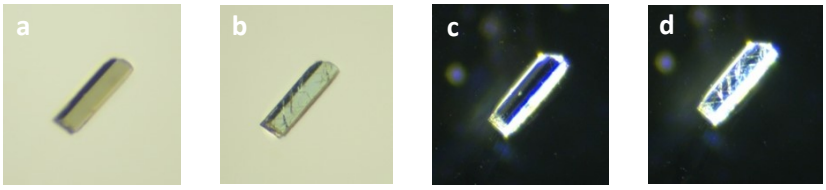

Figure S21. The crystal from which data corresponding to **1-Form-III_RT** and **1-Form-III'_RT** were obtained. Images were observed by optical microscopy in a light (**a**, **b**) and dark (**c**, **d**) field. This series of photographs shows the photosalient effect using a 10-Watt light source before UV-light irradiation (**a**, **c**) and after 30 seconds of UV-light irradiation (**b**, **d**).

7 Further Discussion

7.1 *1-Form-III as an Intermediate Polymorph*

1-Form-III can be viewed as an intermediate form between previously published **1-Form-I** and **1-Form-II** because of (i) structure and (ii) material response. The structures of **1-Form-I**, **1-Form-III**, and **1-Form-II** contain either 0, 1, or 2 4-naphthylvinylpyridine ligands where the olefins are aligned and within Schmidt's criteria (4.2 Å), respectively. Structurally, we see a progression of the criteria required for a photomechanical response.

Additionally, the observed photomechanical responses are also indicative of **1-Form-III** being an intermediate form. Where as **1-Form-I** displays dramatic fragmentation and jumping, **1-Form-II** displays no photomechanical response at all. This can be viewed as the PSE being turned "on" and "off". **1-Form-III** displays a PSE that is intermediate of this. Its photosalient behaviour is muted relative to that of **1-Form-I**, but dramatically enhanced relative to that of **1-Form-II**.

7.2 *UV Experiments and Photochemical Conversion of 1-Form-III' to Compound 2*

All crystal growth occurred in the dark. Suitable crystals were quickly examined under the microscope light before being screened on the diffractometer. Once a suitable crystal was found, a full data set was collected in the dark (lights in the diffractometer and X-ray facility were turned off). This procedure was done during data collection of **1-Form-III_RT** and **1-Form-III_LT**. Once data collection was complete, the corresponding crystal was taken off the diffractometer and exposed to 10-Watt UV light for 30 seconds. During this time period, the PSE had begun and ceased (see Figure 2 and Figure S13). The crystal was remounted for data collection at either room temperature (**1-Form-III'_RT**) or low temperature (**1-Form-III'_LT**) under light free conditions.

Despite our best efforts at ensuring the crystals were not exposed to light for extended periods of time, some light exposure during screening and mounting of the crystals was necessary. We suspect that the ~5-10 min exposure to light from the microscope resulted in a small amount conversion of our initial forms (**1-Form-III_RT** and **1-Form-III_LT**)[1] to the partially dimerized forms (**1-Form-III'_RT** and **1-Form-III'_LT**). The conversion ratios of 14% and 16%, respectively, were determined by modelling and refining the "disordered component" of the structure. It is important to note that even though a small percentage of the photodimerized product was identified crystallographically, NMR spectroscopy of the crystals did not show significant conversion (**Figure S8**). This supports our hypothesis that broad-spectrum light of the microscope resulted in a small degree of photodimerization. Despite this, no observable macroscopic effect was observed until the crystals were exposed to the UV light source (~365 nm).

[1] The CIF of **1-Form-I** displays evidence of unmodelled disorder due to partial photodimerization, however this was not discussed in the original manuscript [ref. 6].

Data indicates that **1-Form-III'_RT** underwent the PSE after only 26% conversion, whereas **1-Form-III'_LT** underwent the PSE after 54%. Conversion of **1-Form-I** was not discussed in the original manuscript, however our analysis of the CIF (modelling both crystallographic parts) of their partial structure indicates conversion of 54%.

8 References

1. Bruker Biospin. TopSpin Software Version 4.0.7. **2017**, Karlsruhe, Germany: Bruker Biospin GmbH.
2. PANalytical. X'Pert Data Collector Software (Version 5.3.0.62) **2015**, Almelo, Netherlands: PANalytical B.V.
3. Agilent. CrysAlis PRO. **2014**, Agilent Technologies Ltd, Yarnton, Oxfordshire, England.
4. Dolomanov, O. V., Bourhis, L. J., Gildea, R. J., Howard, J. A. K., & Puschmann, H. *J. Appl. Crystallogr.* **2009**, *42*, 339–341.
5. Moffat, J. G. D., Pham-Tran, V. N. P., Marczenko, K. M. *Can. J. Chem.* **2024**, In Press.
6. Khan, S., Dutta, B., Naaz, S., Choudhury, A., Cazade, P. A., Kiely, E., Guerin, S. Medishetty, R., Mir, M. H. *Commun. Chem.* **2023**, *6*, 150.
7. Yan, B., Jia, X., Sun, S., Zhou, Z., Fang, C., Chen, N., Li, Y. Li, Y., Ma, H. A. *IJRMHM*, **2015**, *48*, 56-60.
8. R. A. Mayo, K. M. Marczenko, E. R. Johnson, *Chem. Sci.* 2023, **14**, 4777.